


ORIGINAL ARTICLE

OPEN

The co-location of MARCO+ tumor-associated macrophages and CTSE+ tumor cells determined the poor prognosis in intrahepatic cholangiocarcinoma

Guangyu Fan^{1,2}  | Changcheng Tao³  | Lin Li⁴  | Tongji Xie^{1,2}  |
 Le Tang^{1,2}  | Xiaohong Han^{5,6,7,8} | Yuankai Shi^{1,2}

¹Department of Medical Oncology, National Cancer Center/National Clinical Research Center for Cancer, Cancer Hospital, Chinese Academy of Medical Sciences & Peking Union Medical College, Beijing, China

²Beijing Key Laboratory of Clinical Study on Anticancer Molecular Targeted Drugs, Beijing, China

³Department of Hepatobiliary Surgery, National Cancer Center/National Clinical Research Center for Cancer, Cancer Hospital, Chinese Academy of Medical Sciences & Peking Union Medical College, Beijing, China

⁴Department of Pathology, National Cancer Center/National Clinical Research Center for Cancer, Cancer Hospital, Chinese Academy of Medical Sciences & Peking Union Medical College, Beijing, China

⁵Clinical Pharmacology Research Center, Peking Union Medical College Hospital, Chinese Academy of Medical Sciences & Peking Union Medical College, Beijing, China

⁶NMPA Key Laboratory for Clinical Research and Evaluation of Drug, Beijing, China

⁷Beijing Key Laboratory of Clinical PK & PD Investigation for Innovative Drugs, Beijing, China

⁸State Key Laboratory of Complex Severe and Rare Diseases, Beijing, China

Correspondence

Yuankai Shi, Department of Medical Oncology, National Cancer Center/National Clinical Research Center for Cancer, Cancer Hospital, Chinese Academy of Medical Sciences & Peking Union Medical College, Beijing Key Laboratory of Clinical Study on Anticancer Molecular Targeted Drugs, No. 17, Panjiayuan Nanli, Chaoyang District, Beijing 100021, China.
 Email: syunkai@cicams.ac.cn

Xiaohong Han, Clinical Pharmacology Research Center, Peking Union Medical College Hospital, Chinese Academy of Medical Sciences & Peking Union Medical College, State Key Laboratory of Complex Severe and Rare Diseases, NMPA Key Laboratory for Clinical Research and Evaluation of Drug, Beijing Key Laboratory of Clinical PK & PD Investigation for Innovative Drugs, No. 1, Shuaifuyuan, Dongcheng District, Beijing 100730, China.
 Email: hanxiaohong@pumch.cn

Abstract

Background and Aims: Intratumor immune infiltration plays a crucial role in interacting with tumor cells in intrahepatic cholangiocarcinoma (ICC). However, the specific phenotypes of immune cells and their spatial distribution within the tumor microenvironment remain unclear. This study aimed to address these limitations by providing a detailed analysis of immune infiltration patterns in ICC using combined spatial and single-cell transcriptomic data.

Approach and Results: We analyzed 29,632 spots from 6 spatial transcriptomic samples and 21,158 cells from 35 single-cell samples of ICC. Two distinct immune infiltration patterns were identified: macrophage+ (characterized by CD68 and macrophage receptor with collagenous structure [MARCO]) and plasma cell+ (characterized by IGHG1 and JCHAIN). These patterns showed contrasting impacts on patient survival, with macrophage+

Abbreviations: CNV, copy number variation; DEGs, differentially expressed genes; EMT, epithelial-to-mesenchymal transition; ICC, intrahepatic cholangiocarcinoma; IGHG, immunoglobulin heavy constant gamma; MARCO, macrophage receptors with collagenous structure; TAM, tumor-associated macrophage; TF, transcription factor; TME, tumor microenvironment.

Guangyu Fan, Changcheng Tao, and Lin Li contributed equally to this work and as co-first authors.

Supplemental Digital Content is available for this article. Direct URL citations are provided in the HTML and PDF versions of this article on the journal's website, www.hepjournal.com.

This is an open access article distributed under the terms of the Creative Commons Attribution-Non Commercial-No Derivatives License 4.0 (CCBY-NC-ND), where it is permissible to download and share the work provided it is properly cited. The work cannot be changed in any way or used commercially without permission from the journal.

Copyright © 2024 The Author(s). Published by Wolters Kluwer Health, Inc.

infiltration associated with poorer outcomes and plasma cell+ infiltration linked to better survival. MARCO+ tumor-associated macrophages (TAMs) were the predominant cell type in macrophage+ samples, indicative of an immune-resistant microenvironment. In MARCO+ TAMs, elevated epithelial-mesenchymal transition activity, angiogenesis, and hypoxia were observed. Spatial transcriptomics and bulk data also revealed co-location of MARCO+ TAMs with cathepsin E (CTSE+) tumor cells, a finding validated by multiplex immunofluorescence in 20 ICC samples. The co-location area was enriched with protumorigenic pathways and suppressed immune responses, and CTSE expression was associated with intrahepatic metastasis and vascular invasion. High infiltration of both MARCO+ TAMs and CTSE+ tumor cells correlated with the poorest survival outcomes. Within the co-location area, the galectin signaling pathway, particularly the LGALS9-CD44 ligand-receptor pair, was highly active in cell-cell communication.

Conclusions: This study identifies 2 intratumor immune infiltration patterns, macrophage+ and plasma cell+, in ICC. Furthermore, the co-location of MARCO+ TAMs and CTSE+ tumor cells contributes to an immune-resistant microenvironment, highlighting potential targets for therapeutic intervention in ICC.

Keywords: immunosuppression, intratumor immune infiltration, single-cell sequencing, spatial patterns, spatial transcriptomics

INTRODUCTION

Intrahepatic cholangiocarcinoma (ICC) is the second most common type of liver cancer, with a 5-year survival rate of <20%.^[1] The TOPAZ-1 trial, conducted in 2022, investigated the impact of adding durvalumab, an immunotherapy drug that targets programmed death-ligand 1, to the combination of gemcitabine and cisplatin for the treatment of biliary tract cancer.^[2,3] The results showed a significant improvement in survival without a significant increase in side effects.^[2,3] Following this trial, the three-drug combination has now been established as the preferred initial treatment, marking significant progress in the management of biliary tract cancer. Nevertheless, immunotherapy shows limited clinical effectiveness, achieving a long-lasting response in around 25% of biliary tract patients.^[4,5] Current understanding suggests that these difficulties mostly stem from the immunosuppressive tumor microenvironment (TME).^[6] However, our comprehension of the TME in ICC and its role in promoting immune resistance to checkpoint inhibition and other immunotherapies is still limited.

The TME comprises various host cells, such as cancerous cells, immune cells, and stromal cells, as well as noncellular elements, including secreted substances and extracellular proteins.^[7] These factors

collectively play significant roles in the development, progression, and spread of cancer, as well as in the response to immune checkpoint blockade therapy. Within the TME, the presence of immune cells infiltrating the tumor is crucial, as these cells interact with tumor cells, leading to either favorable (antitumor) or unfavorable (protumor) outcomes. Although the TME in ICC is critical, existing research has primarily focused on specific markers or cell types, such as PD-L1 expression and CD8 T-cell infiltration.^[8,9] These studies have shown significant variation and limited consensus. Additionally, historical depictions of the TME have often been subjective, relying on immunohistochemical staining and bulk transcriptomics data without a thorough investigation of cell composition and interactions.^[10,11] The complex relationships between immune cells infiltrating the tumor and tumor cells have not been fully understood, partly because of the crucial role of tumor cells in modifying the immunophenotype of the TME. Gaining a more detailed and nuanced understanding of these interactions is essential for improving our knowledge of ICC and for developing better treatment approaches that specifically target the TME.

Traditional bulk-level transcriptomics data cannot distinguish between distinct cell types. On the other hand, single-cell RNA sequencing, though valuable, is

limited in its ability to consider spatial context, making it difficult to study the connections between the local environment and specific interactions between cells. However, advancements in spatial transcriptomics technology have provided powerful tools to analyze the exact spatial distribution of genes.^[12,13] This enables researchers to understand how tumor-intrinsic features interact with other critical cell types in the context of tumor formation and therapeutic response. Spatial transcriptomics allows for the detailed analysis of the molecular and cellular composition of immune infiltration within tumors. It also facilitates the study of these interactions with surrounding components of the TME while maintaining the integrity of tissue architecture. This technology provides a comprehensive understanding of the TME, paving the way for the development of more effective, targeted treatments.

In this study, we leveraged spatial transcriptomics to characterize the phenotype of intratumor immune infiltration in ICC. We identified 2 distinct infiltration patterns: macrophage+ and plasma cell+. Moreover, we recognized macrophage receptors with collagenous structure (MARCO)+ tumor-associated macrophages (TAMs) as the primary cell type in macrophage+ samples, indicating an immune-resistant microenvironment. The co-location of MARCO+ TAM and cathepsin E (CTSE)+ tumor cells was observed in spatial transcriptomics data and validated by multiplex immunofluorescence performed on 20 ICC samples. Both MARCO+ TAM and CTSE+ tumor cells were associated with worse survival, highlighting their potential as therapeutic targets. In conclusion, our study sheds light on intratumor immune infiltration in ICC and identifies the co-location of MARCO+ TAM and CTSE+ tumor cells as contributors to immune resistance.

METHODS

Ethical Compliance and Patient Consent

This study was conducted in accordance with the Declaration of Helsinki and the Declaration of Istanbul. The research protocol was approved by the Independent Ethics Committee of the National Cancer Center/Cancer Hospital, Chinese Academy of Medical Sciences, and Peking Union Medical College (Approval No. 23/262-4004). All patients provided written informed consent prior to sample collection.

Patient Samples

Seventy formalin-fixed paraffin-embedded ICC samples and 8 fresh ICC samples were obtained from pretreatment patients at the National Cancer Center/Cancer Hospital, Chinese Academy of Medical Sciences, and Peking Union Medical College. Sample collection

followed institutional ethical guidelines, and each sample was collected with informed consent from the respective patient. The staging of samples was assessed by certified pathologists in accordance with the American Joint Committee on Cancer (AJCC) criteria.

Data and materials

Single-cell data from GSE125449, GSE138709, GSE151530, and GSE181878 were sourced from the Gene Expression Omnibus database.^[14–17] Clinical data and metadata were taken from the original studies. The study included 21,158 cells from 35 ICC tumor samples. Transcriptomics data and clinical information of the FU-ICCA cohort were obtained from a published study, encompassing 255 patients with ICC.^[18]

Clustering analysis of spatial transcriptomics

Spatial transcriptomics data underwent clustering analysis using Seurat. Spots with fewer than 500 detected genes or >6000 genes and those with over 20% mitochondrial counts were filtered out. Gene expression was adjusted using Seurat SCT normalization algorithm. Principal component analysis-based dimension reduction was performed, extracting the first 20 principal components for Louvain clustering to define cell types at a resolution of 0.8. Uniform Manifold Approximation and Projection is a dimension reduction technique used to visualize high-dimensional data in a lower-dimensional space, typically two or three dimensions. Uniform Manifold Approximation and Projection was used for visualizing high-dimensional data in two or three dimensions.

Differential expression analysis and gene set enrichment analysis

Differentially expressed gene (DEG) analysis within each cluster was conducted using the Seurat package's FindAllMarkers function, with parameters `min.pct = 0.1` and `logfc.threshold = 0.25`. Gene set enrichment analyses were performed using the R package `fgsea` to elucidate the biological functions of identified DEGs in each cluster. The analysis included enrichment assessments in cancer hallmark, Biological Process Gene Ontology, and Kyoto Encyclopedia of Genes and Genomes gene sets.

Dimension reduction and clustering analysis for single-cell data

The top 2000 most variable genes were identified using the `FindVariableFeatures` function and subsequently

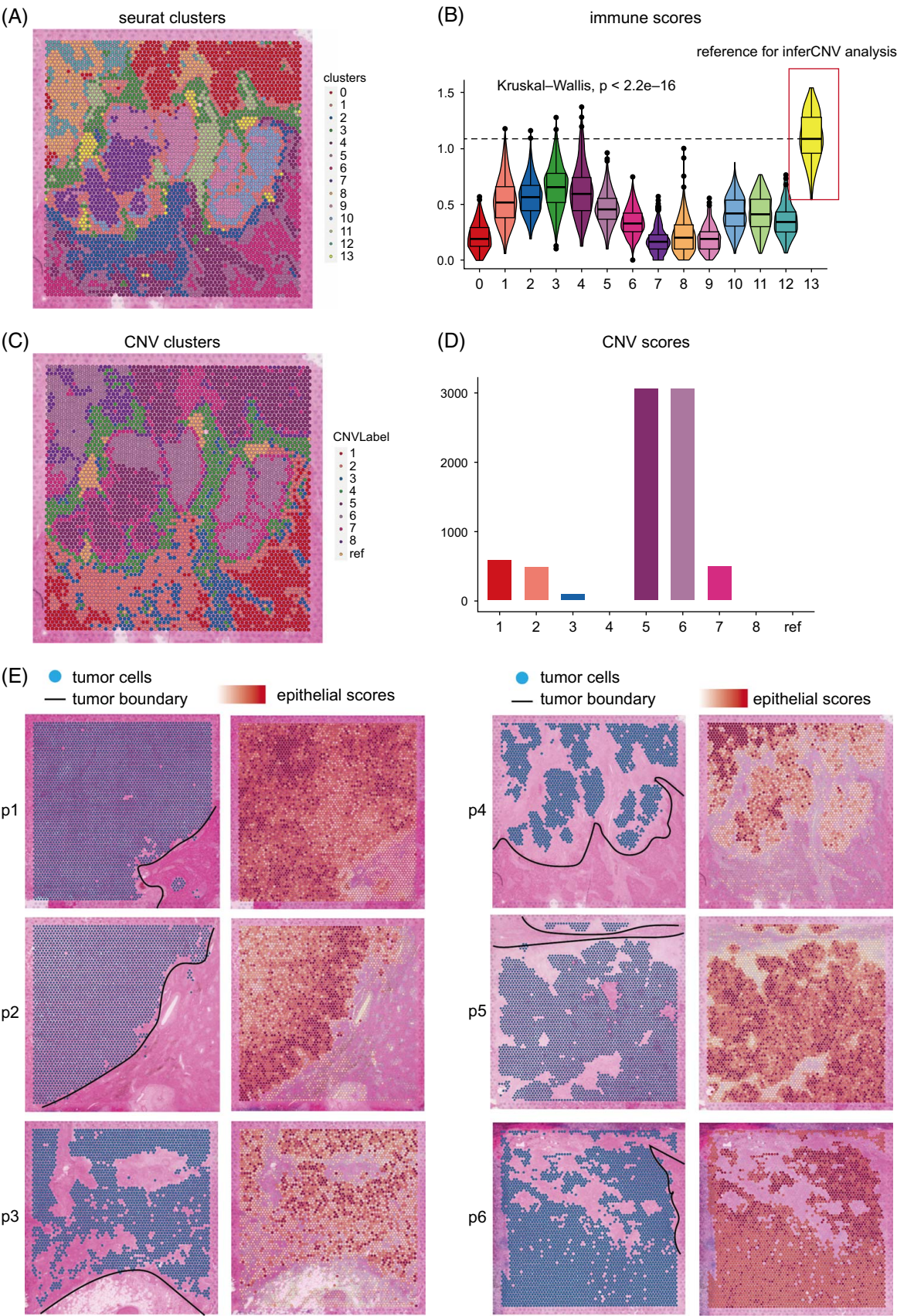


FIGURE 1 The identification of malignant cells in spatial transcriptomics data. (A) Clustering of 4873 spots in patient 4 (p4) into 13 distinct clusters. (B) Distribution of immune score in the 13 clusters. (C) Hierarchical clustering assigning all spots in p4, except the reference cluster, into 8 clusters. (D) Bar charts showing the distribution of copy number variation (CNV) score in the nine clusters. (E) The plot depicted the identified tumor cells, the tumor boundary, and the distribution of tumor-specific epithelial scores in 6 tumor samples. Abbreviation: CNV, copy number variation.

employed for principal component analysis within the Seurat package. To mitigate batch effects within the data sets, we applied the Harmony algorithm from the Harmony R package before conducting the clustering analysis. Cell subtypes were identified through the FindNeighbors and FindCluster functions. Cells were annotated using curated markers, including epithelial cells (EPCAM, KRT8, KRT19), fibroblasts (COL1A1, COL1A2, DCN), endothelial cells (PLVAP, VWF, PECAM1), T cells (CD3D, CD3E, TRAC), B cells (MS4A1, CD79A), and myeloid cells (CD14, CD163, CD68, FCGR3A).

Transcription factor analysis

Transcription factor (TF) activity was inferred using the Dorothea database, which contains signed TF-target interactions (<https://saezlab.github.io/dorothea>).^[19] To construct TF regulons, we used the “dorothea regulon human” wrapper function from the DoRothEA package and selected high-confidence TFs at levels “A,” “B,” and “C.” The run_viper function was then employed to calculate the activities of the regulons. In the context of single-cell data, we constructed regulons based on the mRNA expression levels of each TF and its direct targets. We combined the VIPER algorithm with DoRothEA package using the run_viper function to estimate TF activities from the Dorothea regulons.

Survival analysis

For the survival analyses, patient tissue samples were divided into 2 groups, namely high and low. This categorization was performed using the surv_cutpoint function within the R survminer package. Kaplan-Meier survival curves, measuring the fractions of patients living for a certain time, were then generated to compare the groups and evaluate the influence of the specific genes on prognosis. The statistical significance of the observed differences was assessed using the log-rank test.

Cell-cell communication analysis

CellChat software was used to infer, analyze, and visualize intercellular communication interactions between cell subsets at the single-cell level and spatial transcriptomics level.^[20]

Statistical analysis

The Mann-Whitney *U* test was performed to analyze the differences between the 2 groups. Spearman correlation test was used to assess the correlations between 2 variables. A two-tailed *p*-value of 0.05 was considered statistically significant. R 4.1.0 was used for the entire data processing, statistical analysis, and plotting procedures.

RESULTS

The identification of malignant cells in spatial transcriptomics data

To examine the spatial arrangement of ICC, spatial transcriptomic sequencing was performed on tumor tissue sections obtained from 6 patients with ICC. Comprehensive quality information for the 6 spatial transcriptomics samples is available in Supplemental Figure S1, <http://links.lww.com/HEP/I711> and Supplemental Table S1, <http://links.lww.com/HEP/I711>.

First, inferCNV analysis was conducted to differentiate malignant cells from other cell types by examining their copy number variation (CNV) patterns. This procedure involved 2 clustering stages. The first stage focused on identifying reference cells for the inferCNV pipeline. An “immune score” was determined for each spot by evaluating a set of immune-related signatures, including pan-immune markers (protein tyrosine phosphatase, receptor type C, pan-T-cell markers (CD2, CD3D, CD3E, CD3G), B-cell markers (CD79A, MS4A1, CD79B), and myeloid cell markers (CD68, CD14). The immune score represents the average level of immune infiltration within each spot. The cluster with the highest immune score was used as the reference for the inferCNV analysis. In patient 4 (p4), 4873 spots were categorized into 13 clusters, with cluster 13 exhibiting the highest immunological score and selected as the reference cluster for inferCNV analysis (Figure 1A, B).

The second clustering step aimed to differentiate malignant cells from other cell types by analyzing CNV patterns. The R package inferCNV used hierarchical clustering with tree partitioning to assign all spots, except for the reference cluster, into 8 clusters (Figure 1C). Clusters 5 and 6, which had exceptionally high CNV values, were identified as malignant clusters. The other clusters had lower CNV scores (Figure 1D). The accuracy of these annotations was confirmed by 2 pathologists who examined the histology material using

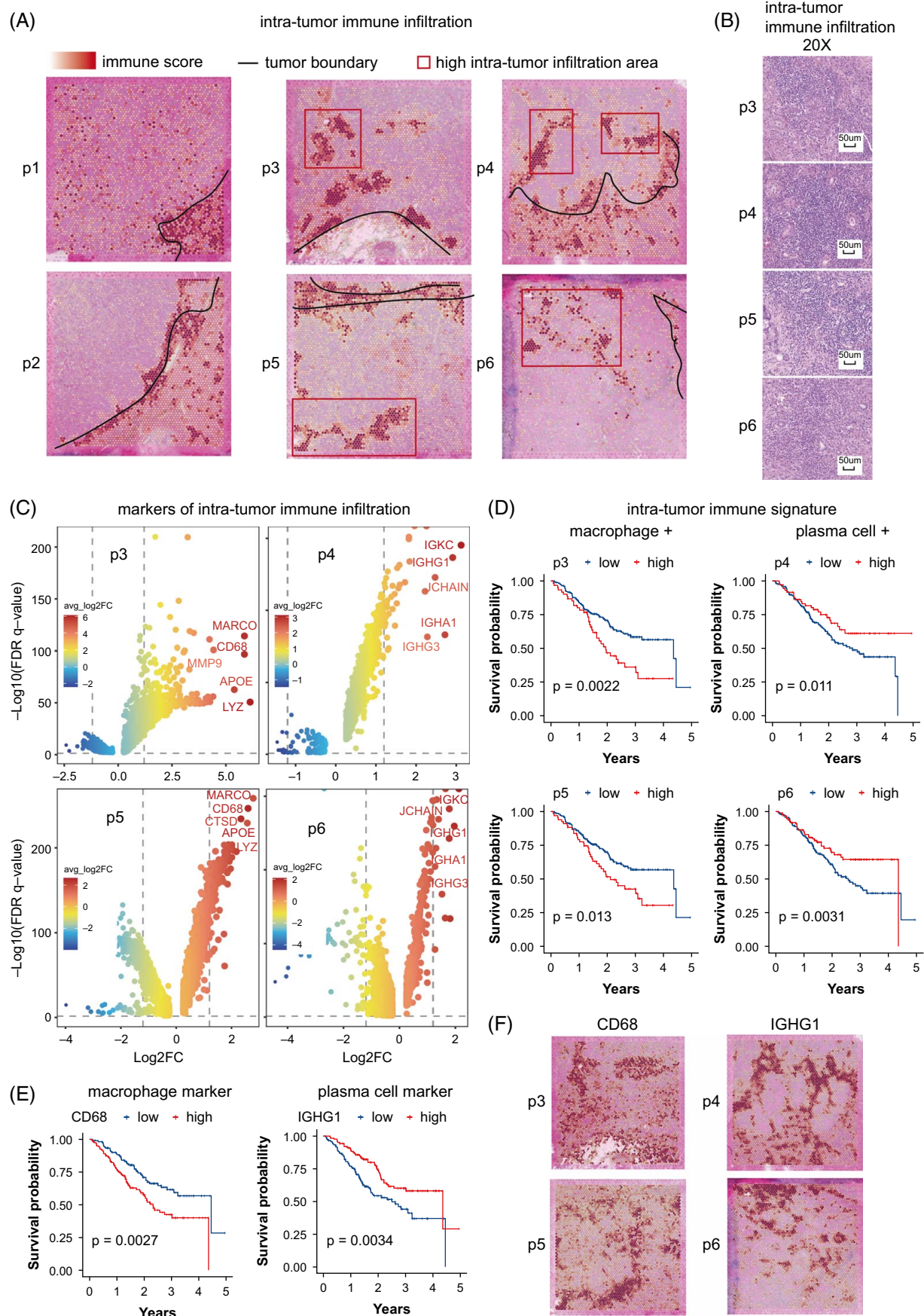


FIGURE 2 Macrophage+ and plasma cell+ intratumor immune infiltration patterns in intrahepatic cholangiocarcinoma (ICC). (A) The plot depicted the tumor boundary, the distribution of immune score, and the high intratumor immune infiltration area in 6 ICC samples. (B) The corresponding HE images of p3 to p5 displayed the infiltrated immune clusters observed from spatial transcriptomics data. (C) The differentially expressed genes (DEGs) of the immune clusters in p3 to p5, respectively. (D) The role of infiltrated immune signature (top 50 DEGs) of p3 to p5 in patients' survival, respectively. (E) CD68 as the macrophage marker and IGHG1 as the plasma cell marker showed adverse and favorable roles in ICC patient survival, respectively. (F) Distribution of the macrophage marker CD68 and the plasma cell marker IGHG1. Abbreviations: APOE, apolipoprotein E; FDR, false discovery rate; IGHG1, immunoglobulin heavy constant gamma 1; LYZ, lysozyme; MARCO, macrophage receptor with collagenous; MMP9, matrix metalloproteinase 9.

hematoxylin-eosin staining of formalin-fixed paraffin-embedded tissue.

The same process was then applied to 5 additional samples, successfully detecting tumor regions in each sample (Figure 1E). All identified tumor cells were located within the tumor regions marked by hematoxylin-eosin histological information. Additionally, the evaluation of tumor-associated epithelial markers (EPCAM, KRT8, KRT19) for each spot in all samples demonstrated that the tumor region had the highest epithelial scores compared to other regions, thus verifying the precise identification of tumor sites.

Macrophage+ and plasma cell+ intratumor immune infiltration patterns in ICC

To explore the immune infiltration landscape in ICC, we assessed the immune score in each sample, representing the average level of immune infiltration (Figure 2A). Notably, 2 samples (p1 and p2) displayed the exclusion of immune cells from the tumor area, while the remaining 4 samples exhibited significant intratumor immune infiltration clusters. Additionally, 5 samples (p1 to p5) showed a noticeable accumulation of immune cells along the tumor boundary.

The corresponding hematoxylin-eosin images confirmed the clusters of immune cells within the tumor area observed in the spatial transcriptomics data (Figure 2B). We then investigated the specific cell composition of intratumor immune clusters in 4 samples with notable immune infiltration. Using 10X-developed cloupe software, we manually extracted the immune clusters and identified their DEGs (Figure 2C). Two samples (p3 and p5) exhibited higher expression of CD68, a macrophage marker. Plasma cell-related markers (IGHA1, IGHG1, IGHG3, and joining chain of multimeric IgA and IgM) showed high expression in p4 and p6. Samples were categorized into macrophage+ and plasma cell+ based on these patterns. To explore the detailed composition of the intratumor immune infiltration, we used combined single-cell data for cell deconvolution. In samples p3 and p5 with intratumor macrophages, macrophages, fibroblasts, and endothelial cells co-located in the infiltration cluster (Supplemental Figure S2, <http://links.lww.com/HEP/I711>). In samples p4 and p6 with intratumor plasma cells, B cells, and T cells were co-located (Supplemental Figure S2, <http://links.lww.com/HEP/I711>).

We examined the role of these immune infiltration clusters in survival using the top 50 DEGs as signatures (Supplemental Table S2, <http://links.lww.com/HEP/I711>). In a bulk-level transcriptomics cohort, the macrophage+ signature from p3 and p4 was associated with poorer survival, while a higher plasma cell+ signature from p5 and p6 indicated longer overall survival (Figure 2D). CD68 as the macrophage marker and immunoglobulin heavy constant gamma 1 (IGHG1) as the plasma cell marker showed adverse and favorable roles in the survival of patients with ICC, respectively, consistent with the macrophage+ and plasma cell+ signatures (Figure 2E). The spatial distribution of CD68 and IGHG1 was consistent with the immune signatures, validating the 2 immune infiltration patterns in spatial transcriptomics (Figure 2F).

To validate the biological and prognostic significance of the infiltrating macrophage signature, we conducted consensus clustering using the ConsensusClusterPlus package on the FU-iCCA cohort. Clustering identified 2 distinct subpopulations among the patients (Supplemental Figure S3A, <http://links.lww.com/HEP/I711>). Cluster 1 (C1) showed higher expression of the genes in the infiltrating macrophage signature compared to cluster 2 (C2) (Supplemental Figure S3B, <http://links.lww.com/HEP/I711>). Patients in C1 had worse survival outcomes than those in C2, reinforcing the prognostic value of the infiltrating macrophage signature (Supplemental Figure S3C, <http://links.lww.com/HEP/I711>). C1 also showed enrichment in pathways related to proliferation (cell cycle and DNA replication) and protumor features, including activation of TGFB signaling, VEGF signaling, and extracellular matrix remodeling (Supplemental Figure S3D, <http://links.lww.com/HEP/I711>). Conversely, C2 demonstrated a robust immune response marked by pathways involved in leukocyte migration and inflammatory responses (Supplemental Figure S3D, <http://links.lww.com/HEP/I711>). These findings align with our spatial and single-cell data analyses, supporting the protumor role of MARCO+ macrophages.

MARCO+ TAM was the primary cell type in the macrophage+ samples

MARCO was highly expressed in macrophage+ samples, and patients with ICC with high MARCO levels had

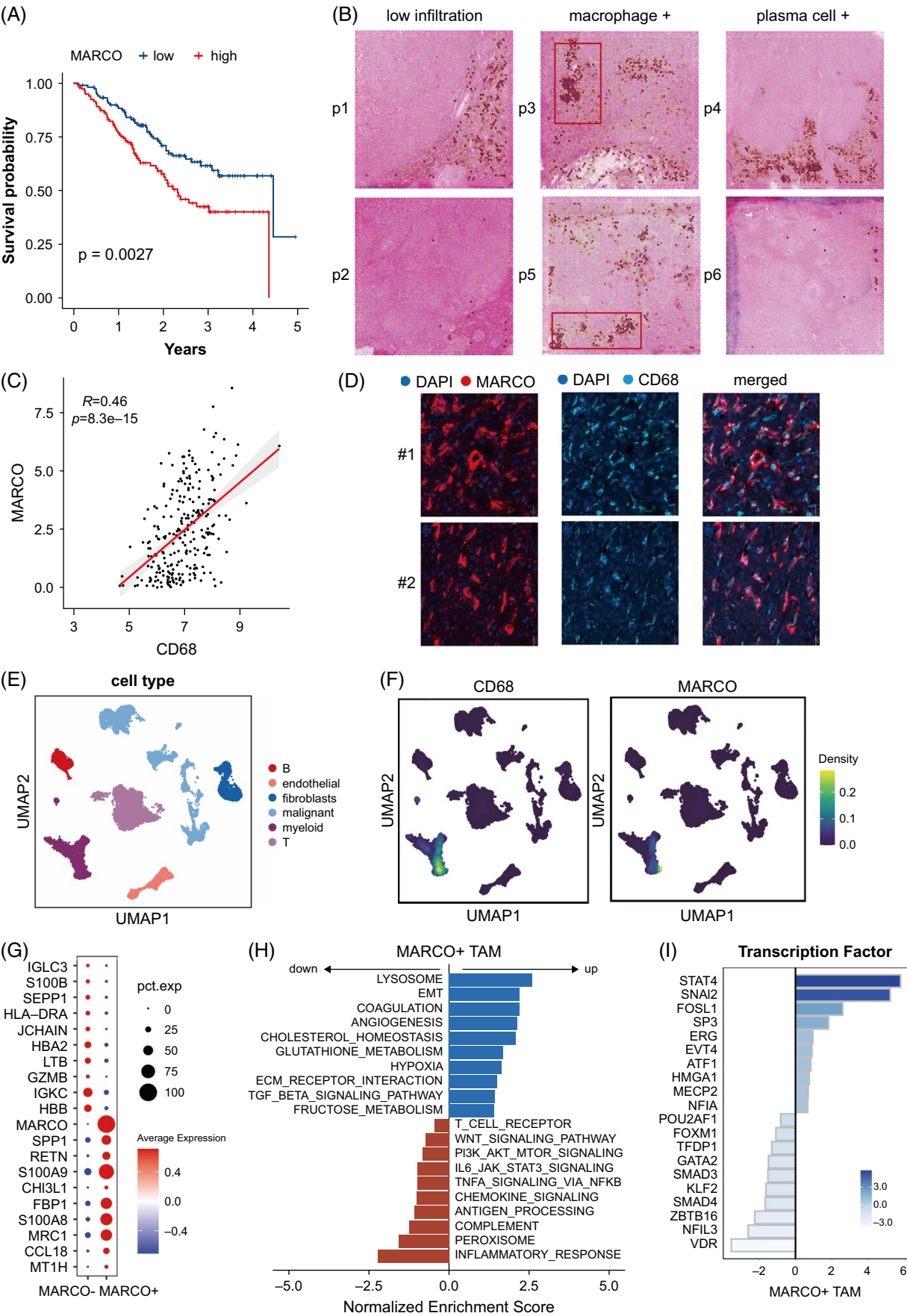


FIGURE 3 MARCO+ tumor-associated macrophage (TAM) in the macrophage+ samples correlated with worse prognosis. (A) Patients with intrahepatic cholangiocarcinoma (ICC) with high MARCO levels had shorter overall survival (OS) time. (B) Distribution of MARCO in samples with distinct immune infiltration patterns. (C) The plot displayed the correlation between MARCO and CD68 in the bulk transcriptomics data. (D) The multiplex immunofluorescence performed in 20 patients with ICC demonstrated the co-location between MARCO and CD68. (E) The single-cell data set was divided into 6 main clusters: malignant cells, myeloid cells, fibroblasts, endothelial cells, T cells, and B cells. (F) Distribution of CD68 and MARCO in single-cell data set. (G) The top 10 upregulated genes in MARCO+ and MARCO- TAM. (H) Bar chart displaying the upregulated and downregulated pathways in MARCO+ TAM. (I) Expression patterns of the most varied transcription factors (TFs) in MARCO+ TAM. Abbreviations: ECM, extracellular matrix; EMT, epithelial-to-mesenchymal transition; MARCO, macrophage receptor with collagenous; TAM, tumor-associated macrophage.

shorter overall survival, indicating its adverse role in clinical outcomes (Figure 3A). Thus, we further explored MARCO's phenotype in ICC.

MARCO was highly expressed in the tumor area of macrophage+ samples while mainly expressed in the tumor boundary of low intratumor immune infiltration and plasma cell+ samples (Figure 3B). Detailed visual representations of macrophages (CD68 and CD14), CD68, MARCO, plasma cells (CD79A, CD79B, joining chain of multimeric IgA and IgM, and (IGHG1)), and IGHG1 across 4 patients are in Supplemental Figure S4, <http://links.lww.com/HEP/I711>. The correlation between MARCO and CD68 was 0.46 in bulk transcriptomics data, indicating MARCO as a reliable macrophage marker in ICC (Figure 3C). To validate MARCO at the protein level, we performed multiplex immunofluorescence in 20 patients with ICC using CD68 to annotate macrophages. MARCO co-located with CD68, indicating its role as a marker of immunosuppressive TAM (Figure 3D).

To investigate MARCO's phenotype accurately, we used large-scale single-cell data sets (GSE125449, GSE138709, GSE151530, GSE181878, and our sequenced 8 ICC samples).^[14–17] Clinical and quality information of the 8 ICC samples sequenced by single-cell technology is in Supplemental Table S3, <http://links.lww.com/HEP/I711>. Six main clusters were identified: epithelial cells, myeloid cells, fibroblasts, endothelial cells, T cells, and B cells (Figure 3E). Myeloid cells comprised 7.3% of the total cell population, with 15.8% of these being MARCO+ TAMs. The distribution of MARCO in TAM validated its role as a typical macrophage marker and a subset of CD68+ TAM (Figure 3F). Comparing MARCO+ and MARCO- TAM, we compiled a list of DEGs (Figure 3G). Notably, SPP1, RETN, and FBP1 were highly expressed in MARCO+ TAM, promoting tumor cell proliferation and suppressing immune response.^[21–23] S100A9 and S100A8, Ca²⁺ binding proteins, were also upregulated in MARCO+ TAM.^[24]

Pathway analysis revealed increased epithelial-to-mesenchymal transition (EMT) activities in MARCO+ TAM, involving extracellular matrix remodeling and promoting tumor metastasis (Figure 3H). Enhanced angiogenesis and hypoxia were observed in MARCO+ TAM. The immune-suppressing pathway TGFB signaling was also enhanced in MARCO+ TAM. Changes in

metabolism-related pathways, including cholesterol homeostasis and glutathione metabolism, were noted. Conversely, immune-related pathways (tumor necrosis factor alpha signaling, antigen binding, chemokine signaling pathway, complement, and inflammatory response) were suppressed in MARCO+ TAM.

We further examined the role of TFs in promoting the aggressive phenotype of MARCO+ TAM (Figure 3I). Enhanced regulon activities of STAT4, promoting macrophage activation and macrophage-CD8+ T-cell cross talk, were observed. SNAI2, an EMT TF, and FOSL1, associated with EMT and cancer cell stemness, exhibited heightened regulon activities in MARCO+ TAM.^[25–27]

MARCO+ TAMs had immunosuppressive effects on TME in ICC

We curated classical M2-like macrophage markers, including CD206 and CD301.^[28] Using a panel of panCK, MARCO, CD206, and CD301 for multiplex immunofluorescence on 10 ICC samples, we found that MARCO+ TAMs also expressed CD206 and CD301, indicating their M2-like characteristics (Figure 4A).

To explore secreted protein profiles, we identified MARCO+ and MARCO- TAMs from single-cell data. We examined 92 proteins involved in tumor immunity, chemotaxis, vascular and tissue remodeling, apoptosis, and autophagy using the OLINK immuno-oncology assay.^[29] VEGFA and TGFB1 were significantly higher in MARCO+ TAMs, suggesting immunosuppressive properties (Figure 4B and Supplemental Figure S5, <http://links.lww.com/HEP/I711>). Multiplex immunofluorescence on ICC samples using PanCK, MARCO, VEGFA, and TGFB1 showed MARCO co-located with VEGFA and TGFB1, reinforcing the immunosuppressive nature of MARCO+ TAMs (Figure 4C, D).

Analyzing combined scRNA-seq data sets, we divided samples into high and low MARCO+ TAM groups based on the median number of MARCO+ TAMs. The high MARCO+ TAM group showed a higher proportion of malignant cells and myeloid cells, with fewer T and B cells (Figure 4E). Multiplex immunofluorescence on ICC samples using MARCO, CD3, and CD8 revealed areas with high MARCO expression had less CD3 and CD8 expression, highlighting the

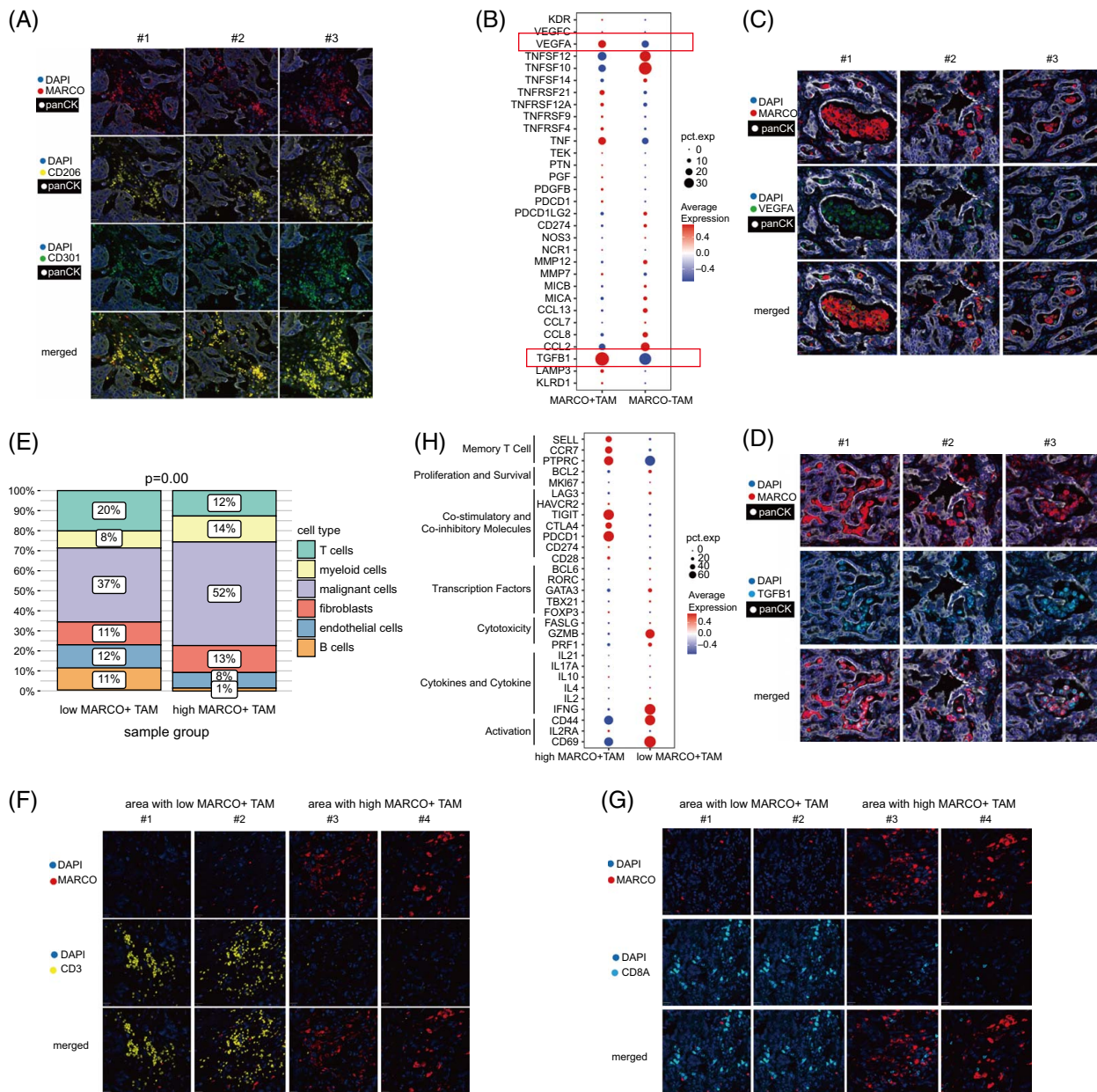


FIGURE 4 MARCO+ tumor-associated macrophage (TAM) had immunosuppressive effects on tumor microenvironment in intrahepatic cholangiocarcinoma (ICC). (A) The multiplex immunofluorescence performed in patients with ICC demonstrated the co-expression between MARCO, CD206, and CD301. (B) The distribution of 31 proteins from the OLINK immuno-oncology assay in MARCO+ TAMs and MARCO- TAMs. (C) The multiplex immunofluorescence performed in patients with ICC indicated that MARCO demonstrated co-location with VEGFA. (D) The multiplex immunofluorescence performed in patients with ICC demonstrated the co-location of MARCO with TGFBI. (E) The proportion of 6 main clusters (malignant cells, myeloid cells, fibroblasts, endothelial cells, T cells, and B cells) in samples with high MARCO+ TAMs and with low MARCO+ TAMs. (F) The multiplex immunofluorescence performed in patients with ICC demonstrated that areas with high MARCO expression had less CD3 expression. (G) The multiplex immunofluorescence performed in patients with ICC demonstrated that areas with high MARCO expression had less CD8 expression. (H) The distribution of genes involved in T-cell function, including activation, differentiation, effector functions, and exhaustion in samples with high MARCO+ TAMs and with low MARCO+ TAMs. Abbreviations: MARCO, macrophage receptor with collagenous; TAM, tumor-associated macrophage.

immunosuppressive effect on T cells and CD8 T cells (Figure 4F, G).

We curated genes relevant to T-cell activities, including activation, differentiation, effector functions, and exhaustion. High MARCO+ TAM samples exhibited higher

expression of memory T-cell markers like SELL and CCR7 and increased expression of immune checkpoints PDCD1, CTLA4, and TIGIT. Conversely, low MARCO+ TAM samples showed higher expression of cytokines like IFNG and cytotoxicity markers like GZMB (Figure 4H).

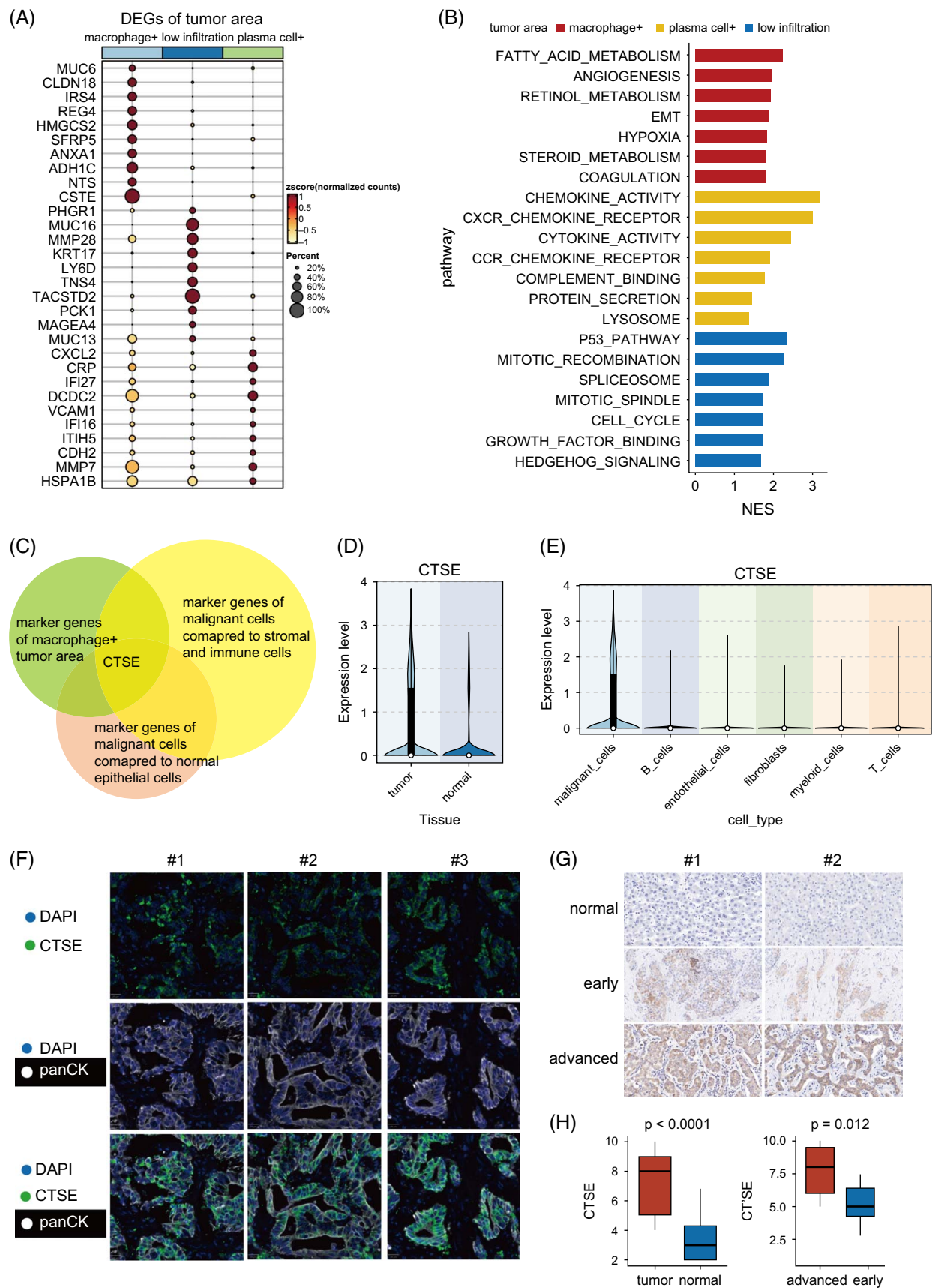


FIGURE 5 CTSE was highly expressed in tumor areas with infiltrated MARCO+ tumor-associated macrophage (TAM). (A) The differentially expressed genes (DEGs) of tumor cells in samples with distinct immune infiltration patterns. (B) Pathway analysis unveiled distinct biological activities in 3 types of tumor areas. (C) CTSE was identified as the potential tumor marker correlating with the infiltrated MARCO+ TAM. (D) CTSE exhibited elevated expression in tumor cells compared to normal epithelial cells. (E) CTSE exhibited elevated expression in tumor cells compared to immune cells and stromal cells. (F) The multiplex immunofluorescence performed in 20 patients with ICC demonstrated the main expression of CTSE in tumor cells. (G) Immunohistochemistry images of CTSE in our cohort consisting of 70 patients with ICC. (H) Boxplots displaying the distribution of CTSE in normal, early, and advanced-stage samples. Abbreviations: CTSE, cathepsin E; WT, wild type.

CTSE was highly expressed in tumor areas with infiltrated MARCO+ TAM

Tumor cells can remodel the immune components in the TME to facilitate immune evasion, tumor growth, metastasis, and therapeutic resistance.^[11] We investigated tumor cell phenotypes in samples with different intratumor immune infiltration patterns to uncover potential tumor-immune interactions as targets for ICC immunotherapy.

We calculated the DEGs of tumor areas in samples with distinct immune infiltration patterns (Figure 5A and Supplemental Table S6, <http://links.lww.com/HEP/I711>). ANXA1, linked to EMT and promoting the M2 macrophage phenotype, was a key DEG.^[30] TACSTD2, a stem cell marker, was upregulated in low intratumor infiltration areas, correlating with poor immunogenic response.^[31] CXCL2 and CRP, immune-related genes associated with inflammation and immune response, were highly expressed in plasma cell+ tumor areas.

Pathway analysis revealed distinct activities in different tumor areas (Figure 5B). Macrophage+ tumor areas showed increased EMT activities, angiogenesis, hypoxia, and enhanced metabolism-related pathways. Plasma cell+ tumor areas had enriched immune response pathways, including chemokine signaling. Tumor areas with low intratumor infiltration were characterized by upregulated proliferation-related pathways.

We aimed to identify tumor-specific genes inducing MARCO+ TAM infiltration and exerting immunosuppressive effects. Using large-scale single-cell data sets, we extracted marker genes distinctive to tumor cells compared to immune and normal epithelial cells, with criteria of $\text{avg_log2FC} > 0.25$ and $p\text{-value} < 0.05$ (Figure 5C). CTSE was identified, showing the highest expression in macrophage+ tumor areas (Figure 5C). CTSE exhibited elevated expression in tumor cells compared to immune and normal epithelial cells (Figure 5D, E). To validate CTSE expression at the protein level, we performed multiplex immunofluorescence in 20 patients with ICC using panCK antibody to annotate tumor cells. CTSE was mainly expressed in tumor cells compared to adjacent normal areas (Figure 5F). Immunohistochemistry in 70 patients with ICC confirmed elevated CTSE expression in tumor cells, with higher levels in patients with advanced ICC compared to early-stage patients (Figure 5G, H).

The co-location of CTSE+ tumor cells and MARCO+ TAM worsens the prognosis of patients with ICC

We examined the spatial expression patterns of CTSE in 3 immune infiltration types of samples (Figure 6A). CTSE was predominantly expressed in tumor cells rather than normal epithelial and immune/stromal cells, aligning with single-cell analysis. In macrophage+ samples (p3 and p5), CTSE showed notable expression within tumor areas. In low intratumor infiltration and plasma cell+ samples, CTSE had significantly lower expression levels.

To validate this, we calculated the correlation of CTSE with macrophage+ immune infiltration markers (CD68 and MARCO) in a large ICC patient cohort (Figure 6B). CTSE and CD68 had a correlation of 0.32, while CTSE and MARCO had a correlation of 0.49, indicating a stronger association with MARCO macrophages. Multiplex immunofluorescence staining of CTSE and MARCO in 20 ICC patient samples confirmed the co-location of CTSE+ tumor cells and MARCO+ macrophages (Figure 6C).

Analyzing 249 patients with ICC with whole-exome and mRNA sequencing data, we focused on mutations in KRAS, IDH1, IDH2, and TP53.^[32–35] Both CTSE and MARCO expressions were higher in KRAS and TP53 mutation groups, suggesting interaction specificity between MARCO+ TAMs and CTSE+ ICC cells in these mutations (Figure 6D). CTSE showed higher expression in wild-type IDH1 and IDH2 groups, while MARCO expression did not differ significantly between mutation and wild-type groups for these genes.

CTSE was highly expressed at the tumor boundary, defined as the nearest two-spot width area near the tumor's outermost circle (Figure 6E, F). In a large ICC cohort with bulk transcriptomics data, CTSE was higher in the vascular invasion group and associated with intrahepatic metastasis^[18] (Figure 6G). However, it is important to note the considerable phenotypic variability within these groups, as indicated by the range of CTSE expression levels observed in the box plots. Patients with high CTSE levels had shorter overall survival, consistent with its immunosuppressive role. Patients with high levels of both CTSE and MARCO had the worst clinical outcomes, indicating a potential protumor interaction between the 2 cell types (Figure 6H).

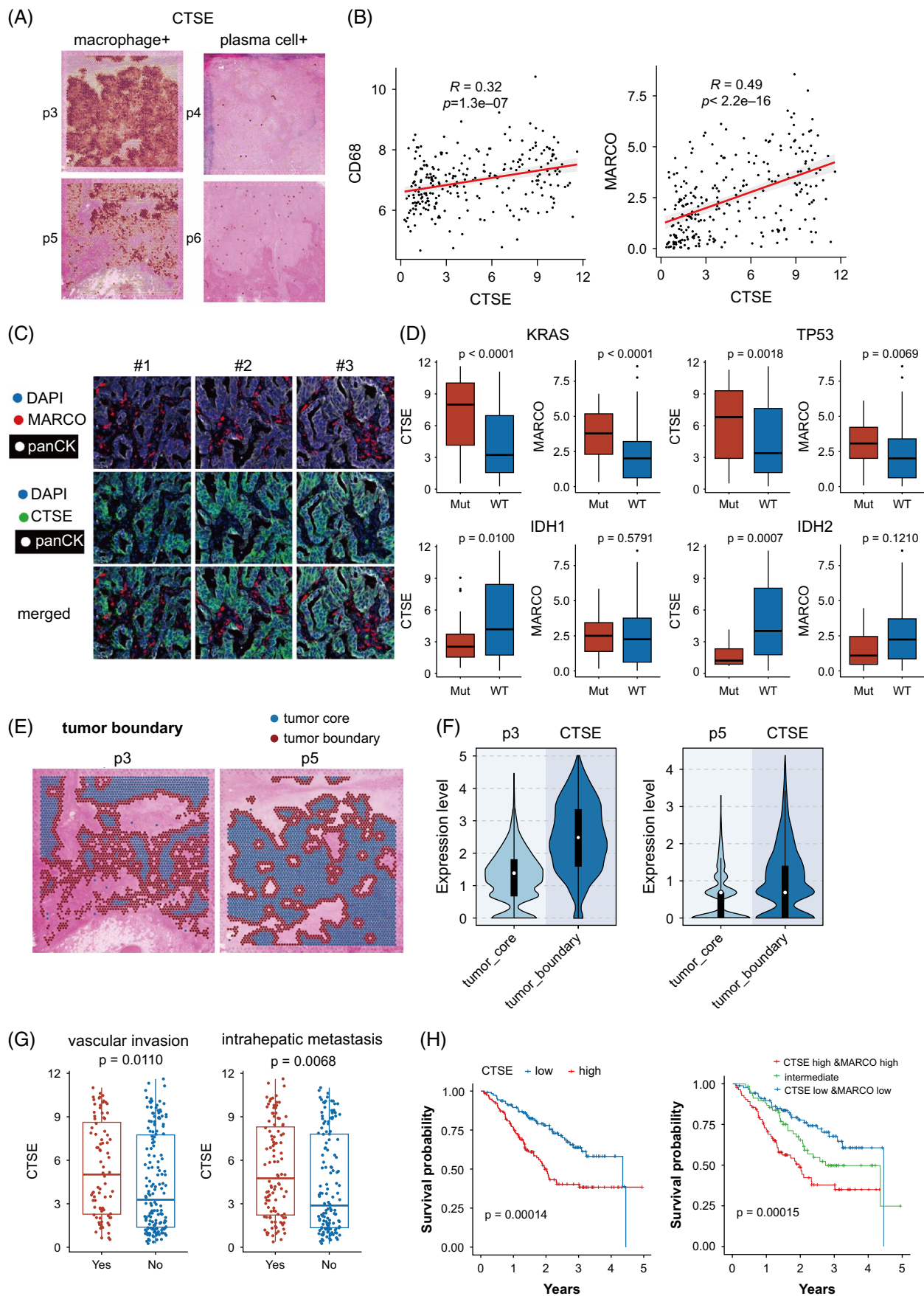


FIGURE 6 The co-location of CTSE+ tumor cells and MARCO+ TAM was revealed by spatial transcriptomics. (A) The spatial expression patterns of CTSE in 3 immune infiltration types of samples. (B) The correlation of CTSE and macrophage+ immune infiltration markers (CD68 and MARCO) in the bulk transcriptomics data. (C) The multiplex immunofluorescence performed in 20 patients with ICC demonstrated the co-location of CTSE+ tumor cells and MARCO+ macrophage in ICC tumor area. (D) The relationship between the distribution of CTSE and MARCO and specific genetic mutations (KRAS, IDH1, IDH2, TP53, BRAF, and EGFR). (E) The tumor boundary is defined as the nearest two-spot width area near the outermost circle of the tumor area. (F) The tumor boundary had higher expression levels of CTSE. (G) CTSE exhibited associations with vascular invasion and intrahepatic metastasis. (H) Patients with high CTSE levels had shorter OS time, and with both high CTSE and high MARCO levels displayed worst clinical outcome. Abbreviations: CTSE, cathepsin E; IDH2, isocitrate dehydrogenase 2; MARCO, macrophage receptor with collagenous; WT, wild type.

Cell-cell communication between MARCO+ TAM and CTSE+ tumor cells

We investigated cell-cell communication between MARCO+ TAM and CTSE+ tumor cells to understand their interaction and their role in immune suppression. The 10X Genomics Visium platform's limitation in cell resolution necessitated evaluating their cross talk at the single-cell level (Figure 7A). Our analysis identified the GALECTIN pathway, where LGALS9 from CTSE+ tumor cells activated CD44, CD45, and HAVCR2 on MARCO+ TAM. LGALS9, known for its immune inhibitory role, was central in this interaction. We also identified MIF, MK, and LAMININ signaling in CTSE+ tumor cells, associated with cancer hallmarks such as growth and metastasis. The intercellular adhesion molecule pathway played a role in both the self-communication of MARCO+ TAM and their interaction with CTSE+ cells, promoting stemness and chemotherapy resistance.

At the spatial transcriptomics level, focusing on the macrophage+ sample p3, we observed 5 nontumor clusters, with N3 and N4 as immune infiltration clusters (Figure 7B). LGALS9 from the tumor area activated CD44 in N3 and N4, where MARCO+ TAMs accumulated (Figure 7C). The GALECTIN pathway had the highest communication activity strength (Figure 7D). Multiplex immunofluorescence on 20 ICC tumor samples confirmed LGALS9 as a secretory protein from CTSE+ tumor cells, activating CD44 on MARCO+ TAMs (Figure 7F).

CellChat analysis on single-cell data showed that LGALS9+ tumor cells had more extensive communication with other cell types than LGALS9- tumor cells, especially with MARCO+ TAMs, suggesting that LGALS9+ tumor cells primarily influence MARCO+ TAMs, rather than T cells (Figure 7G). This interaction underscores the immunosuppressive role of LGALS9 in the TME, particularly affecting MARCO+ TAMs.

DISCUSSION

The presence of immune cells within a tumor is crucial for modulating the immune response against the tumor. The impact of these immune cells on the TME varies depending on the cell types involved. Although examining intratumor immune infiltration and its spatial arrangement in ICC is challenging, this study provided a comprehensive

analysis, revealing macrophage+ and plasma cell+ populations. MARCO+ TAMs were identified as the predominant cell type in macrophage+ samples, strongly associated with CTSE+ tumor cells. These findings can guide future clinical trials and identify potential biomarkers for prognosis and treatment strategies.

We observed 2 distinct immune infiltration patterns in ICC: macrophage-positive and plasma cell-positive. TAMs, constituting over 50% of the tumor-infiltrating cells, can be categorized into proinflammatory M1-like and immunosuppressive M2-like types.^[36] MARCO, a scavenger receptor involved in pattern recognition, is consistently expressed on M2-like macrophages and linked to poorer prognosis. In preclinical models, anti-MARCO monoclonal antibodies reduce tumor sizes and shift MARCO-expressing TAMs from an M2 to an M1 phenotype, while decreasing regulatory T cells.^[37] In melanoma, combining anti-PD-L1 antibodies with anti-MARCO antibodies in tumor-bearing mice led to NK cell and CD8+ T-cell migration, highlighting MARCO's potential as an immunotherapy target.^[38]

Our study also examined tumor characteristics leading to MARCO+ TAM invasion. CTSE, an aspartic protease from the peptidase A1 family, was abundantly expressed in the tumor region alongside MARCO+ TAMs. CTSE is a crucial proteolytic enzyme in cancer development, with suggestions to use cysteine cathepsin inhibitors as anticancer treatments.^[39,40] CTSE is excessively expressed in pancreatic ductal adenocarcinoma and gastric cancer, correlating with tumor metastasis.^[39,40] Suppression of CTSE significantly reduced the self-renewal capacity of HCC cells in vitro.^[41] The importance of CTSE in maintaining stemness was validated by tumor formation experiments in immunodeficient animals. An anti-CTSE nano-drug showed potential in improving treatment effectiveness for pancreatic ductal adenocarcinoma.^[42]

Our research uncovered the spatial convergence of MARCO+ TAMs and CTSE+ tumor cells and explored their intercellular interactions. LGALS9 emerged as a crucial checkpoint activated by CTSE+ tumor cells, which inhibits immune cells. LGALS9, expressed at higher levels in tumor cells compared to surrounding tissues, is linked to tumor development and progression.^[43] It suppresses the immune system by promoting regulatory T cells and reducing Th17 and Th1 cells, thus controlling excessive immune responses and inflammation.^[44,45]

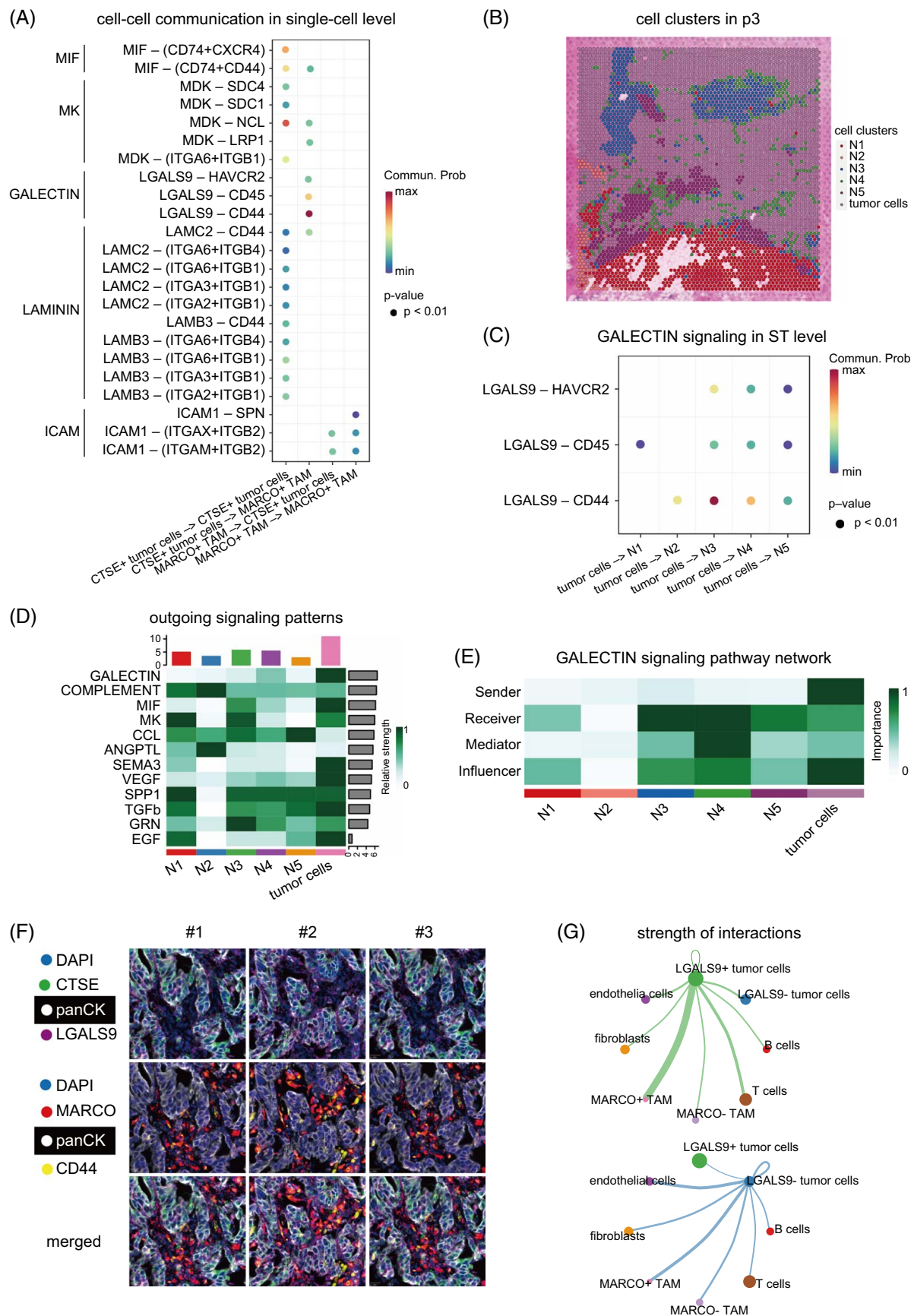


FIGURE 7 Cell-cell communication between MARCO+ TAM and CTSE+ tumor cells. (A) The cell-cell communication between MARCO+ TAM and CTSE+ tumor cells at the single-cell level. (B) The cell clusters in sample p3. (C) The ligand-receptor pairs in GALECTIN signaling pathway signaled from tumor cells to other clusters. (D) The outgoing pattern of all cell clusters. (E) The GALECTIN signaling pathway network. (F) The multiplex immunofluorescence image revealed the LGALS9-CD44 ligand-receptor pair in the cell-cell communication MARCO+ TAM and CTSE+ tumor cells. (G) The interaction strengths between T cells/ MARCO+ TAMs and LGALS9+ tumor cells/LGALS9- tumor cells. Abbreviations: CTSE, cathepsin E; MARCO, macrophage receptor with collagenous; TAM, tumor-associated macrophage.

In our study, MARCO+ TAMs co-localized with CTSE + tumor cells and expressed CD44. We identified the LGALS9-CD44 signaling pathway as highly active in their interaction zone, suggesting that CTSE-secreting LGALS9 could influence tumor progression. This co-localization indicates that TAMs receiving LGALS9 via CD44 might support tumor cells, potentially creating a microenvironment that enhances tumor survival and spread. CTSE may aid in remodeling the extracellular matrix, boosting tumor cell invasiveness, while MARCO + TAMs might support this process through cytokine secretion and matrix remodeling. The active LGALS9-CD44 pathway could further facilitate tumor progression and immune evasion by enhancing cell-cell communication and adhesion.

Future research should address the limitations of our study, including the lack of immunotherapy-treated patients. We plan to validate our findings by constructing mouse models with manipulated MARCO expression and using ICC mouse cell lines to generate CTSE+ tumor cells. Co-culture experiments will assess interactions and changes in cell behavior. We will manipulate Gal9 expression in CTSE+ cells to observe effects on MARCO+ cells and use CRISPR-Cas9 to generate Gal9 knockout cell lines for further validation. These studies will help elucidate the role of the Gal9-CD44 pathway and identify potential therapeutic targets.

CONCLUSIONS

This study demonstrated the characterization of intra-tumor infiltration patterns in ICC and thoroughly elucidated the co-location of MARCO+ TAM and CTSE+ tumor cells that induced immunosuppressive TME.

DATA AVAILABILITY STATEMENT

The raw sequence data reported in this paper have been deposited in the Genome Sequence Archive in the National Genomics Data Center, China National Center for Bioinformatics/Beijing Institute of Genomics, Chinese Academy of Sciences (GSA:HRA006757).

AUTHOR CONTRIBUTIONS

Conception/design: Yuankai Shi, Xiaohong Han; methodology: Guangyu Fan, Changcheng Tao, Lin Li, and Tongji Xie; formal analysis: Guangyu Fan, Lin Li, and Tongji Xie; writing—manuscript writing: Guangyu Fan, Changcheng Tao, Tongji Xie, Lin Li, Le Tang; writing—revising and editing: Yuankai Shi and Xiaohong Han.

FUNDING INFORMATION

This study was supported by the National Science and Technology Major Project for Key New Drug Development (2017ZX09304015 and 2019ZX09201-002).

CONFLICTS OF INTEREST

The authors have no conflicts to report.

ORCID

Guangyu Fan  <https://orcid.org/0000-0003-1561-0007>

Changcheng Tao  <https://orcid.org/0000-0002-1082-2572>

Lin Li  <https://orcid.org/0000-0002-4932-6488>

Tongji Xie  <https://orcid.org/0000-0002-3276-9645>

Le Tang  <https://orcid.org/0000-0002-5192-3329>

REFERENCES

- Spolverato G, Kim Y, Alexandrescu S, Marques HP, Lamelas J, Aldrighetti L, et al. Management and outcomes of patients with recurrent intrahepatic cholangiocarcinoma following previous curative-intent surgical resection. *Ann Surg Oncol*. 2016;23:235–43.
- Moris D, Palta M, Kim C, Allen PJ, Morse MA, Lidsky ME. Advances in the treatment of intrahepatic cholangiocarcinoma: An overview of the current and future therapeutic landscape for clinicians. *CA Cancer J Clin*. 2023;73:198–222.
- Oh D-Y, Lee KH, Lee DW, Yoon J, Kim TY, Bang JH, et al. Gemcitabine and cisplatin plus durvalumab with or without tremelimumab in chemotherapy-naïve patients with advanced biliary tract cancer: An open-label, single-centre, phase 2 study. *Lancet Gastroenterol Hepatol*. 2022;7:522–32.
- Kawamura E, Matsubara T, Kawada N. New era of immune-based therapy in intrahepatic cholangiocarcinoma. *Cancers*. 2023;15:3993.
- Zayac A, Almhanna K. Hepatobiliary cancers and immunotherapy: Where are we now and where are we heading? *Transl Gastroenterol Hepatol*. 2020;5:8.
- Merters J, Lamarca A. Integrating cytotoxic, targeted and immune therapies for cholangiocarcinoma. *J Hepatol*. 2023;78:652–7.
- Li D, Lin S, Hong J, Ho M. Immunotherapy for hepatobiliary cancers: Emerging targets and translational advances. *Adv Cancer Res*. 2022;156:415–49.
- Ahn S, Lee Y, Kim JW, Lee JC, Hwang JH, Yoon YS, et al. Programmed cell death ligand-1 (PD-L1) expression in extrahepatic biliary tract cancers: A comparative study using 22C3, SP263 and E1L3N anti-PD-L1 antibodies. *Histopathology*. 2019;75:526–36.
- Zhu Y, Wang XY, Zhang Y, Xu D, Dong J, Zhang Z, et al. Programmed death ligand 1 expression in human intrahepatic cholangiocarcinoma and its association with prognosis and CD8 T-cell immune responses. *Cancer Manag Res*. 2018;10:4113–23.
- Job S, Rapoud D, Dos Santos A, Gonzalez P, Desterke C, Pascal G, et al. Identification of four immune subtypes characterized by distinct composition and functions of tumor microenvironment in intrahepatic cholangiocarcinoma. *Hepatol* (Baltimore, Md). 2020;72:965–81.

11. Xia T, Li K, Niu N, Shao Y, Ding D, Thomas DL, et al. Immune cell atlas of cholangiocarcinomas reveals distinct tumor microenvironments and associated prognoses. *J. Hematol. Oncol.* 2022;15:37.
12. Vickovic S, Eraslan G, Salmén F, Klughammer J, Stenbeck L, Schapiro D, et al. High-definition spatial transcriptomics for in situ tissue profiling. *Nat Methods.* 2019;16:987–90.
13. Ståhl PL, Salmén F, Vickovic S, Lundmark A, Navarro JF, Magnusson J, et al. Visualization and analysis of gene expression in tissue sections by spatial transcriptomics. *Science (New York, NY).* 2016;353:78–82.
14. Chai X, Wang J, Li H, Gao C, Li S, Wei C, et al. Intratumor microbiome features reveal antitumor potentials of intrahepatic cholangiocarcinoma. *Gut Microbes.* 2023;15:2156255.
15. Ma L, Hernandez MO, Zhao Y, Mehta M, Tran B, Kelly M, et al. Tumor cell biodiversity drives microenvironmental reprogramming in liver cancer. *Cancer Cell.* 2019;36:418–430.e6.
16. Zhang M, Yang H, Wan L, Wang Z, Wang H, Ge C, et al. Single-cell transcriptomic architecture and intercellular crosstalk of human intrahepatic cholangiocarcinoma. *J Hepatol.* 2020;73:1118–30.
17. Ma L, Wang L, Khatib SA, Chang CW, Heinrich S, Dominguez DA, et al. Single-cell atlas of tumor cell evolution in response to therapy in hepatocellular carcinoma and intrahepatic cholangiocarcinoma. *J Hepatol.* 2021;75:1397–408.
18. Dong L, Lu D, Chen R, Lin Y, Zhu H, Zhang Z, et al. Proteogenomic characterization identifies clinically relevant subgroups of intrahepatic cholangiocarcinoma. *Cancer Cell.* 2022;40:70–87.e15.
19. Holland CH, Tanevski J, Perales-Patón J, Gleixner J, Kumar MP, Mereu E, et al. Robustness and applicability of transcription factor and pathway analysis tools on single-cell RNA-seq data. *Genome Biol.* 2020;21:36.
20. Jin S, Guerrero-Juarez CF, Zhang L, Chang I, Ramos R, Kuan CH, et al. Inference and analysis of cell-cell communication using CellChat. *Nat Commun.* 2021;12:1088.
21. Grasmann G, Smolle E, Olschewski H, Leithner K. Glucocorticogenesis in cancer cells—Repurposing of a starvation-induced metabolic pathway? *Biochim Biophys Acta Rev Cancer.* 2019;1872:24–36.
22. Sudan SK, Deshmukh SK, Poosarla T, Holliday NP, Dyess DL, Singh AP, et al. Resistin: An inflammatory cytokine with multifaceted roles in cancer. *Biochim Biophys Acta Rev Cancer.* 2020;1874:188419.
23. Matsubara E, Yano H, Pan C, Komohara Y, Fujiwara Y, Zhao S, et al. The significance of SPP1 in lung cancers and its impact as a marker for protumor tumor-associated macrophages. *Cancers.* 2023;15:2250.
24. Chen Y, Ouyang Y, Li Z, Wang X, Ma J. S100A8 and S100A9 in cancer. *Biochim Biophys Acta Rev Cancer.* 2023;1878:188891.
25. Casalino L, Talotta F, Matino I, Verde P. FRA-1 as a regulator of EMT and metastasis in breast cancer. *Int J Mol Sci.* 2023;24:8307.
26. Xiao J, Sun F, Wang YN, Liu B, Zhou P, Wang FX, et al. UBC9 deficiency enhances immunostimulatory macrophage activation and subsequent antitumor T cell response in prostate cancer. *J Clin Invest.* 2023;133:e158352.
27. Zhou W, Gross KM, Kuperwasser C. Molecular regulation of Snai2 in development and disease. *J Cell Sci.* 2019;132:jcs235127.
28. Toledo B, Zhu Chen L, Paniagua-Sancho M, Marchal JA, Perán M, Giovannetti E. Deciphering the performance of macrophages in tumour microenvironment: a call for precision immunotherapy. *J Hematol Oncol.* 2024;17:44.
29. Kartsonaki C, Pang Y, Millwood I, Yang L, Guo Y, Walters R, et al. Circulating proteins and risk of pancreatic cancer: A case-subcohort study among Chinese adults. *Int J Epidemiol.* 2022;51:817–29.
30. Zheng L, Li L, Wang B, Zhang S, Fu Z, Cheng A, et al. Annexin A1 affects tumor metastasis through epithelial-mesenchymal transition: A narrative review. *Translational cancer research.* 2022;11:4416–33.
31. Lenárt S, Lenárt P, Šmarda J, Remšík J, Souček K, Beneš P. Trop2: Jack of all trades, master of none. *Cancers.* 2020;12:3328.
32. Chaisaingmongkol J, Budhu A, Dang H, Rabibhadana S, Pupacdi B, Kwon SM, et al. Common molecular subtypes among Asian hepatocellular carcinoma and cholangiocarcinoma. *Cancer Cell.* 2017;32:57–70.e3.
33. Sia D, Tovar V, Moeini A, Llovet JM. Intrahepatic cholangiocarcinoma: Pathogenesis and rationale for molecular therapies. *Oncogene.* 2013;32:4861–70.
34. Israel MA, Danziger N, McGregor KA, Murugesan K, Gjoerup O, Sokol ES, et al. Comparative genomic analysis of intrahepatic cholangiocarcinoma: Biopsy type, ancestry, and testing patterns. *Oncologist.* 2021;26:787–96.
35. Jolissaint JS, Soares KC, Seier KP, Kundra R, Gönen M, Shin PJ, et al. Intrahepatic cholangiocarcinoma with lymph node metastasis: Treatment-related outcomes and the role of tumor genomics in patient selection. *Clin Cancer Res.* 2021;27:4101–8.
36. Basak U, Sarkar T, Mukherjee S, Chakraborty S, Dutta A, Dutta S, et al. Tumor-associated macrophages: An effective player of the tumor microenvironment. *Front Immunol.* 2023;14:1295257.
37. Georgoudaki A-M, Prokopec KE, Boura VF, Hellqvist E, Sohn S, Östling J, et al. Reprogramming tumor-associated macrophages by antibody targeting inhibits cancer progression and metastasis. *Cell reports.* 2016;15:2000–11.
38. Eisinger S, Sarhan D, Boura VF, Ibarlucea-Benitez I, Tyystjärvi S, Oliynyk G, et al. Targeting a scavenger receptor on tumor-associated macrophages activates tumor cell killing by natural killer cells. *Proc Natl Acad Sci USA.* 2020;117:32005–16.
39. Palermo C, Joyce JA. Cysteine cathepsin proteases as pharmacological targets in cancer. *Trends Pharmacol Sci.* 2008;29:22–8.
40. Cruz-Monserrate Z, Abd-Elgaliel WR, Grote T, Deng D, Ji B, Arumugam T, et al. Detection of pancreatic cancer tumours and precursor lesions by cathepsin E activity in mouse models. *Gut.* 2012;61:1315–22.
41. Ho DW, Tsui YM, Sze KMF, Chan LK, Cheung TT, Lee E, et al. Single-cell transcriptomics reveals the landscape of intra-tumoral heterogeneity and stemness-related subpopulations in liver cancer. *Cancer Lett.* 2019;459:176–85.
42. Li H, Wang P, Deng Y, Zeng M, Tang Y, Zhu WH, et al. Combination of active targeting, enzyme-triggered release and fluorescent dye into gold nanoclusters for endomicroscopy-guided photothermal/photodynamic therapy to pancreatic ductal adenocarcinoma. *Biomaterials.* 2017;139:30–8.
43. Lv Y, Ma X, Ma Y, Du Y, Feng J. A new emerging target in cancer immunotherapy: Galectin-9 (LGALS9). *Genes & diseases.* 2023;10:2366–82.
44. Zhu C, Anderson AC, Schubart A, Xiong H, Imitola J, Khoury SJ, et al. The im-3 ligand galectin-9 negatively regulates T helper type 1 immunity. *Nat Immunol.* 2005;6:1245–52.
45. Seki M, Oomizu S, Sakata K, Sakata A, Arikawa T, Watanabe K, et al. Galectin-9 suppresses the generation of Th17, promotes the induction of regulatory T cells, and regulates experimental autoimmune arthritis. *Clin Immunol.* 2008;127:78–88.

How to cite this article: Fan G, Tao C, Li L, Xie T, Tang L, Han X, et al. The co-location of MARCO+ tumor-associated macrophages and CTSE+ tumor cells determined the poor prognosis in intrahepatic cholangiocarcinoma. *Hepatology.* 2025;82:25–41. <https://doi.org/10.1097/HEP.0000000000001138>